Chinese Chemical Letters 37 (2026) 112463

Contents lists available at ScienceDirect

Chinese Chemical Letters

journal homepage: www.elsevier.com/locate/cclet

Synergistic dual-functional photocatalysis for hydrogen production simultaneously with pollutant degradation and value-added compound production

Hao Bi[a], Guang Yang[b], Qian Liu[a], Ran Zhao[a], Fangyuan Chen[a,*], Zhurui Shen[a,*]

[a] School of Materials Science and Engineering, National Institute of New Materials Research, Nankai University, Tianjin 300350, China
[b] Nanke Youyi (Tianjin) Technology Co., Ltd., Tianjin 300192, China

ARTICLE INFO

Article history:
Received 29 July 2025
Revised 29 December 2025
Accepted 23 January 2026
Available online 24 January 2026

Keywords:
Photocatalysis
Dual-functional photocatalyst
Hydrogen evolution
Pollutant degradation
Value-added compound production

ABSTRACT

In the context of dwindling energy resources and worsening environmental conditions, the dual-functional photocatalysis for hydrogen production and pollutant degradation has garnered widespread attention. This review systematically summarizes the latest advancements in photocatalytic technology in these two fields. The article first introduces the preparation methods of photocatalysts, focusing on several promising fundamental materials such as graphitic carbon nitride, metal organic frameworks, and metal oxides/sulfides. It also discusses in detail the synthesis methods of these materials, including pyrolysis, wet chemistry, and deposition methods, which are crucial for enhancing the performance of photocatalysts. Next, the article delves into the applications of dual-functional photocatalysts in hydrogen production and pollutant degradation, particularly the mechanisms and effects of simultaneous hydrogen generation and pollutant degradation. It emphasizes the performance and potential of dual-functional catalysts in these two processes, especially how photocatalysts can achieve both hydrogen evolution and pollutant degradation concurrently. Finally, the article looks ahead to future research directions, highlighting the challenges faced by dual-functional catalysts in technological applications, including the source of H atoms in hydrogen production, the common patterns of reaction sites during pollutant degradation, and the differing properties of oxidation products. It also underscores the potential development opportunities by utilizing hydrogen sources from pollutants and optimizing catalyst design.

© 2026 Published by Elsevier B.V. on behalf of Chinese Chemical Society and Institute of Materia Medica, Chinese Academy of Medical Sciences.

1. Introduction

The escalating consumption and rapid depletion of fossil fuels, coupled with their profound ecological consequences, have thrust this issue into the global spotlight. It has become increasingly evident that pursuing sustainable, renewable energy alternatives is not merely desirable but imperative for our future [1,2]. In recent decades, photocatalysis has emerged as a promising technology for efficient solar energy utilization, exhibiting great potential in various fields, including hydrogen evolution reaction (HER) [3], pollutant degradation reaction (PDR) [4], CO_2 reduction (COOR) [5], biomass conversion [6], NO_x abatement [7].

Moreover, the development of dyes and the pharmaceutical industry leads to abundant pollutant emissions, which can dramatically damage the ecosystem of human daily life. Therefore, efficiently disposing of the abundant pollutants, such as dyes (*e.g.*, Rhodamine B, methyl blue [8]), heavy metal ions (*e.g.*, Cr(VI) [9,10]), antibiotics (*e.g.*, tetracycline (TC) [11]), residues of pharmaceuticals and personal care products (PPCPs) in wastewater (such as naproxen [12], toluene [13]), remains a significant challenge [14]. Among the myriad emerging techniques for pollutant degradation, photocatalytic degradation distinguishes itself as a particularly promising approach due to its environmentally friendly and pollution-free characteristics.

Meanwhile, due to its high energy density, clean water emission, and other advantages, hydrogen energy is considered one of the most promising alternatives to fossil fuels. In the past decades, photocatalytic hydrogen evolution gradually became a promising technique for renewable energy conversion, which has been widely studied [15]. However, the efficiency of photocatalytic hydrogen evolution is limited by the catalysts' property, easy recombination of photogenerated charge carriers, and low transfer efficiency, as well as low selectivity of traditional photocatalysts for products, resulting in low photocatalytic activity [16,17]. Furthermore,

* Corresponding authors.
E-mail addresses: chenfangyuan@nankai.edu.cn (F. Chen), shenzhurui@nankai.edu.cn (Z. Shen).

https://doi.org/10.1016/j.cclet.2026.112463
1001-8417/© 2026 Published by Elsevier B.V. on behalf of Chinese Chemical Society and Institute of Materia Medica, Chinese Academy of Medical Sciences.

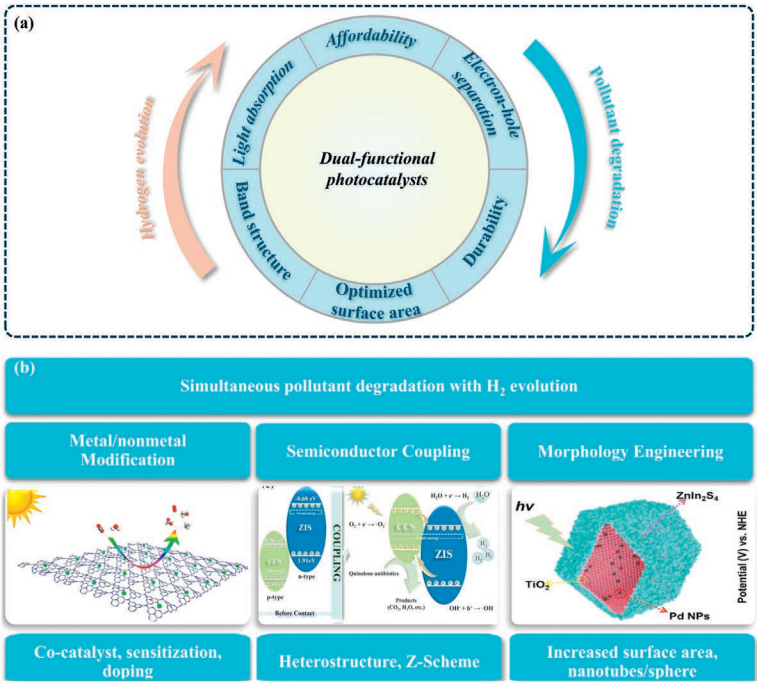


Fig. 1. (a) Schematic representation of the key ideal characteristics of dual-functional photocatalysts. (b) Detailed procedure of dual-functional photocatalysts design for simultaneous organic pollutant degradation and hydrogen evolution. Reprinted with permission [21–23]. Copyright 2021, 2022, 2024, Elsevier.

sacrificial agents, such as methanol, lactic acid, ascorbic acid, and triethanolamine, are commonly used to generate additional electrons to improve the hydrogen evolution rate during photocatalysis. However, these agents are usually toxic and potentially harmful to the environment, and they are expensive, limiting the sustainable development of photocatalytic hydrogen production. Therefore, researchers must focus on sacrificial agent-free photocatalytic systems.

Within this field, photocatalytic degradation, simultaneous with hydrogen evolution, has shown great potential, which has been widely studied. Some researchers demonstrated a sustainable photocatalytic wastewater disposal process, while H_2 is produced, captured, and further utilized [18]. By combining photocatalytic degradation *via* oxidation process with photocatalytic H_2 evolution, heavy metal ion reduction, and CO_2 reduction, *e.g.*, *via* reduction reaction, leads to the improvement of efficiency compared to the pure reaction, which is due to the full utilization of photogenerated electrons and pair holes (h^+) [19]. However, compared to traditional photocatalysts with sacrificial additives, the hydrogen evolution rate of bifunctional photocatalysts still has a relatively significant drawback due to differences in design and functionality [20]. Therefore, it is necessary to design and synthesize efficient dual-functional photocatalysts for further construction of the cooperative hydrogen production system of organic oxidation.

This review aims to enhance our understanding of dual-functional photocatalysts that facilitate hydrogen evolution while simultaneously degrading pollutants (Fig. 1) [21–23]. It summarizes the current advancements in their design, synthesis, and underlying mechanisms.

2. Fundamentals of photocatalysts

Photocatalytic reactions mainly happen at the interface between the photocatalyst's surface area and the liquid phase [24]. Consequently, variations in morphology, size, and crystallinity can significantly impact the physicochemical properties of nanomaterials and the surface chemistry of the photocatalyst, thereby affecting the rate of photocatalytic reactions. Moreover, optimized conductivity is necessary, which will benefit the rapid separation and transmission of photogenerated carriers [25]. As shown in Fig. 1a, ideal dual-functional photocatalysts require affordability, visible-light absorption, durability, suitable band structure, large surface area, and efficient charge separation, while common synthesis strategies are summarized in Fig. 1b and Table S1 (Supporting information).

2.1. g-C_3N_4

At present, g-C_3N_4, with its tri-*s*-triazine framework and diverse N-functionalities, offers H-bonding, tunable basicity, and Lewis acidity crucial for catalysis [26]. Strong metal-support interaction leads to the stability of well-dispersed metal species as isolated single metal atoms for improving selectivity and catalytic activity [27].

Bulky carbon nitride can be obtained *via* thermal conversion of nitrogen-rich precursors such as cyanamide, dicyandiamide, thiourea, urea, and melamine. Also, it can be synthesized through polymerization of nitrogen-rich and oxygen-free precursors (comprising the pre-bonded C-N core structure) by physical vapor deposition (PVD), chemical vapor deposition (CVD), solvothermal method, and solid-state reactions [28]. Due to the 2.7 eV band gap, g-C_3N_4 is capable of carrying photocatalytic activity in the visible light irradiation without additional noble metal for co-catalyst [29]. Over the years, extensive efforts have focused on enhancing g-C_3N_4 to mitigate charge recombination and optimize band structure, using various modification techniques: (1) Structural alterations to optimize performance [30]; (2) Strategic doping to introduce beneficial properties [31,32]; (3) Integration with carbonaceous materials for improved conductivity [33]; (4) Formation of heterojunction composites to facilitate charge separation [34,35].

Wei *et al.* synthesized optimal 2 %Bi/g-C_3N_4, which demonstrated a H_2 evolution rate of 35.9 μmol/h, simultaneous with 5.3 % amoxicillin degradation in 2 h (Figs. 2a-c) [36]. The metallic Bi exhibited the spherical morphology, while the g-C_3N_4 showed the

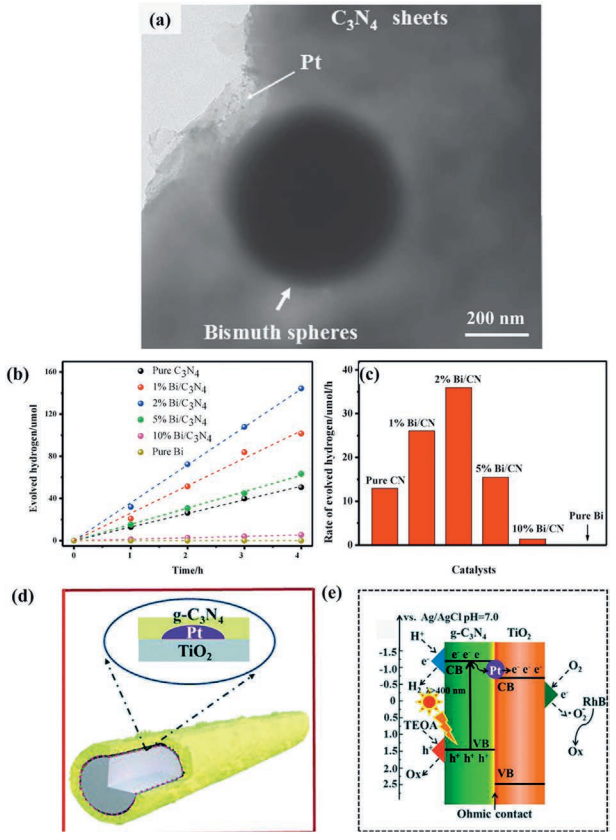


Fig. 2. (a) Scanning electron microscopy (SEM) image of 2 %Bi/C_3N_4. (b) Photocatalytic hydrogen evolution. (c) The rate of hydrogen evolution of C_3N_4 with different Bi loading content. Reprinted with permission [36]. Copyright 2023, Elsevier. (d) Schematic illustration of C_3N_4/Pt/TiO_2 nanowire structures. (e) Illustration of the photo-charges transfer and separation as well as consumption in the RuO_2@TiO_2@Pt during coupled photocatalytic H_2 production and organic pollutant degradation. Reprinted with permission [37]. Copyright 2019, Royal Society of Chemistry.

sheet-like appearance, respectively. The presence of amoxicillin in the reaction acted as a sacrificial reagent, consuming holes and reducing electron-hole recombination, while also providing hydrogen atoms, which significantly enhanced hydrogen production efficiency compared to pure water. These diverse modification strategies aim to overcome the inherent limitations of g-C_3N_4 and further unlock its full potential for various applications in photocatalysis, energy conversion, and environmental remediation. Moreover, Dou *et al.* synthesized the core-shell g-C_3N_4/Pt/TiO_2 nanowire structures with an 8.93 μmol/h H_2 evolution rate in 15 mg/L Rhodamine B (RhB) solution [37]. In this system, g-C_3N_4 forms a core-shell structure with Pt/TiO_2 nanowires (Fig. 2d), where TiO_2 tunes the band structure (Fig. 2e), and Pt promotes heterojunction synergy, enhancing electron transfer and active site generation.

2.2. Metal-organic frameworks (MOFs)

MOFs have been considered as one of the most promising materials presently [38–40]. As depicted in Fig. 3a, MOFs are assembled by metal ions or clusters cooperating with organic ligands, which further extend networks [41]. MOFs' large surface areas and tunable structures enable enhanced light absorption, charge separation, and reactivity, with customizable metal ions, linkers, pore sizes, and functional groups creating abundant, selective active sites for photocatalysis [42]. The MOF-based photocatalysis mechanism involves: (a) Light absorption *via* linkers or photosensitive units to generate electron-hole pairs, (b) efficient separation and transfer of these pairs to active sites, and (c) tailored active sites that facilitate specific reactions through metal or linker modification [5].

However, using MOFs in the field of photocatalysis remained a drawback (Fig. 3b). To solve such a hindrance, engineering of defects, optimization of the calcination time, temperature, and environment, and engineering MOF-derived semiconductors with heterojunctions are always acquired [43]. MOFs are promising dual-functional photocatalysts that simultaneously generate hydrogen from water and oxidize organic molecules, offering a sustainable alternative to toxic sacrificial electron donors. As illustrated in Fig. 3c, Abazari *et al.* synthesized fluorinated MOF(Cu)-NH_2 and further co-catalyzed with Pt nanoparticles for RhB degradation simultaneously with H_2 evolution [44]. The H_2 evolution rate reached 63.64 mmol g^{-1} h^{-1} due to the enhanced visible-light absorption and decrease of electron-hole pair recombination. Besides the support materials, MOFs were also used as the sacrificial reagents for the formation of semiconductors. Kampoiuri *et al.* developed a synthesis strategy for Ti-MOF-derived semiconductors (Figs. 3d and e). X-ray diffusion (XRD) analysis (Figs. 3f and g) showed that Ti-MOF MIL (materials of institute Lavoisier)-125-NH_2 gradually decomposes with increasing temperature, forming amorphous TiO_2 at 400 °C and metastable anatase at 500 °C [45].

2.3. Metal oxides/sulfides

Metal oxides and sulfides, abundant on Earth, are feasible and widely used as photocatalysts (TiO_2, ZrO_2, CdS, MoS_2 and $ZnIn_2S_4$) for energy and environmental applications, with S and O providing coordination sites to stabilize metal atoms [46–51].

TiO_2 is widely used for its stability, durability, low cost, and low toxicity, but its narrow light absorption and high electron-hole recombination limit practical applications [52]. Based on such limitations, many methods have been developed to enhance highly photocatalytic efficiency, such as doping [14], coupling [37], and solid solution of semiconductors [53]. Hu *et al.* synthesized Cu_2O film *via* the electrochemical deposition method, followed by TiO_2 coating on the surface [54]. TiO_2-Cu_2O photocatalysts simultaneously degraded BDE47 (up to 90 % under UV/visible/solar light) and produced H_2 (514.5 μmol/h), with Cu_2O particles of 100-300 nm coated on TiO_2 and a film thickness of 37.65 μm (Figs. 4a and b).

Compared to metal oxides, metal sulfides have narrower band gaps and more sulfur coordination sites [55]. CdS provides tunable vacancies and strong light absorption but suffers from slow charge migration, high carrier recombination, and photo-corrosion, limiting its stability [56,57]. Zhang *et al.* used MoS_2 quantum dots-decorated $ZnIn_2S_4$ on reduced graphene oxide (MoS_2QDs@$ZnIn_2S_4$@RGO) for RhB degradation simultaneously with hydrogen evolution [58]. $ZnIn_2S_4$ sheets grew uniformly on RGO, forming a sheet-on-sheet structure that persisted after MoS_2QDs loading (*d*-spacing 0.27 nm, Figs. 4c-f). The composite achieved H_2 evolution of 45.33 μmol/12 h in RhB and superior RhB degradation, while time-resolved transient photoluminescence (TRPL) showed reduced electron lifetimes (from 75.57 ns to 12.05 ns), indicating faster charge transport (Figs. 4g and h).

In addition to g-C_3N_4, MOFs, and metal oxides/sulfides, various novel materials have demonstrated potential in bifunctional photocatalysis in recent years. These include boron carbonitride (*e.g.*, BCN) [59], metal nitrides (*e.g.*, TiN/TiO) [60], and transition metal carbides (*e.g.*, Mo_2C) [61].

3. Synthesis method

A robust fundamental material is key for efficient bifunctional photocatalysts, with synthesis methods and surface modifications as morphology engineering, metal or nonmetal doping, and semi-

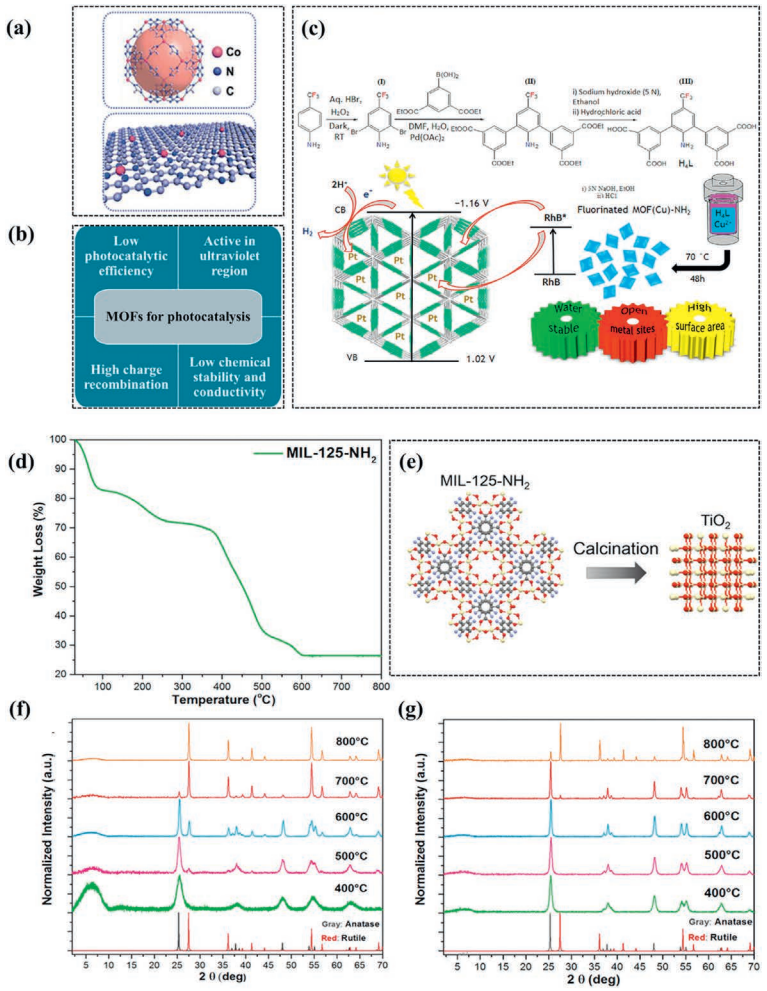


Fig. 3. (a) Schematic illustration of Co MOFs and Co MOFs-derived photocatalyst. Reprinted with permission [41]. Copyright 2019, Wiley. (b) Drawbacks of MOFs for photocatalysis. (c) Synthesis of the fluorinated MOF(Cu)-NH_2 for photocatalytic H_2 evolution and mechanism of dual-functional photocatalysis. Reprinted with permission [44]. Copyright 2023, American Chemical Society. (d) Thermo-gravimetric analysis (TGA) curve of MIL-125-NH_2 obtained under a flow of air at a heating rate of 5 °C/min. (e) Schematic illustration of the synthesis procedure of MIL-125-NH_2-derived TiO_2. (f, g) XRD patterns of the as-synthesized MIL-125-NH_2-derived and TiH_4O_4-derived TiO_2, respectively. (d-g) Reprinted with permission [45]. Copyright 2018, American Chemical Society.

conductor coupling (Table S1), which greatly enhances hydrogen evolution and pollutant degradation [62].

3.1. Pyrolysis from different precursors

Pyrolysis requires different precursors that decompose at elevated temperatures under different atmospheres. In the past decade, a series of heteroatom-doped bifunctional photocatalysts have been synthesized *via* pyrolysis [63,64]. At present, the precursors can be concluded as metal-organic frameworks (MOFs) [65], ZIF-8 (zeolitic imidazolate framework-8) [64], biomass material [66,67], small molecules [68,69], polymers [12,70] and other categories.

As shown in Figs. S1a and b (Supporting information), two typical ways of biomass and g-C_3N_4 as precursors for pyrolysis are schematized, respectively. High temperature leads to enhanced graphitic structure. However, single atoms always acquire high surface energy, which results in sintering and deactivation. Zhang *et al.* synthesized Bi-MOF-derived single metal atom-doped photocatalysis *via* pyrolysis under different temperatures [65]. As shown in Fig. S1c (Supporting information), above 450 °C, surface Bi nanoparticles shrink faster than central ones, and after 500 °C, NH_3 from dicyandiamide (DICY) both accelerates Bi atomization and promotes nitrogen incorporation into the carbon network. Wei *et al.* also reported the same characteristics during the pyrolysis [71]. Increasing pyrolysis temperature and time enlarged nanoparticle size while reducing their number, indicating concurrent sintering and atomization (Figs. S1d and e in Supporting information); this method enables heteroatom-doped photocatalysts, but temperatures above 900 °C may degrade semiconductor carriers.

Oxygen/nitrogen functional groups in GO or CNNTs (carbon nitride nanotubes) are capable of capturing and drafting metal cations [25]. Small molecules are increasingly used as precursors, carbon/nitrogen sources, or ligands for photocatalyst synthesis, with oxygen- and nitrogen-rich organics being preferred, such as phthalocyanine [72], porphyrins [73], and melamine [74]. In the past decade, research has focused on the M-N_x sites, which were generated from coordination between metal ions and N and other heteroatoms [69,71]. Mateen synthesized atomic sites embedded 1D carbon nitride nanotubes (Mo^1@CNNTs) from melamine (Fig. S1f in Supporting information) for TC degradation, simultaneously with hydrogen evolution [75]. Density functional theory (DFT) calculations (Fig. S1g in Supporting information) showed that Mo atoms anchored by pyridinic N atoms in the C/N framework retain geometry and enhance charge transfer, improving photocata-

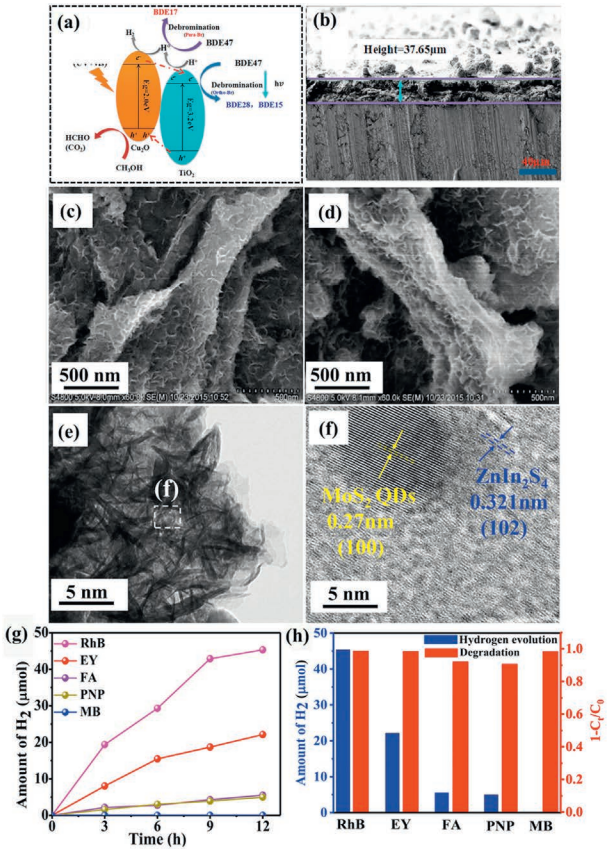


Fig. 4. (a) BDE47 degradation pathway simultaneous with H_2 evolution mechanism. (b) SEM images of Cu_2O film. Reprinted with permission [54]. Copyright 2017, Elsevier. SEM images of (c) $ZnIn_2S_4$@RGO1 and (d) $5MoS_2QDs@ZnIn_2S_4$@RGO1. Transmission electron microscopy (TEM) images of $MoS_2QDs@ZnIn_2S_4$@RGO (e, f). H_2 production and simultaneous pollutant degradation over $MoS_2@ZnIn_2S_4$@RGO under simulated solar light for 12 h: (g) Accumulation of H_2 production, (h) simultaneous H_2 production with pollutant degradation. Reprinted with permission [58]. Copyright 2017, Elsevier.

lyst stability. Similarly, N/C-rich polymers like polymerized PDEB can serve as anchoring matrices [76], polydopamine (PDA) [77], and polyaniline (PANI) [70,78], have been used for synthesis with M-N-C sites.

3.2. Wet chemical method

The wet chemical method, favored for its simplicity, cost-effectiveness, and scalability, enables controllable synthesis and tunable physicochemical properties of metal sulfide photocatalysts through adjustment of process parameters [79]. As shown in Figs. 5a-h, Wang *et al.* synthesized the dual-functional $ZnIn_2S_4@CuCo_2S_4$ photocatalyst for hydrogen evolution from wastewater, which concluded synthesis of $CuCo_2S_4$ as a base material *via* hydrothermal at first, followed by $ZnIn_2S_4$ (ZIS) dispersing on $CuCo_2S_4$ (CCS) [21]. $CuCo_2S_4$ showed a flower-like spherical structure of intersecting nanosheets with particle diameters of approximately 1-2 μm (Fig. 5a). The images after the *in situ* growth of ZIS on CCS (Fig. 5b) revealed that stacked $CuCo_2S_4$ was converted into small na-clusters, followed by adhering to the 2D layer of ZIS. Tao *et al.* synthesized a novel dual-functional 0D $Cd_{0.5}Zn_{0.5}S$/2D Ti_3C_2 hybrid, which was fabricated by a solvothermally *in situ* generated assembling method [80]. As shown in Fig. 5i, 2D Ti_3C_2 was synthesized by LiF/HCl etching of Ti_3AlC_2, followed by *in situ* growth of $Cd_{0.5}Zn_{0.5}S$; their combination formed a Schottky heterojunction that suppressed electron-hole.

3.3. Deposition

Electrochemical deposition is a versatile and effective method for fabricating dual-functional photocatalysts. This technique involves the controlled deposition of metal/nonmetal atoms onto various support materials using electrochemical processes [81].

During the photochemical deposition, metal precursors in solution are reduced to single atoms or nanoparticles under ultraviolet light. In general, there are two pathways for this approach: One is the liquid-phase method, and the other is the solid-phase method. It is worth noting that the preparation process was straightforward for batch preparation. As illustrated in Figs. 5j-n, sheaf-like TiO_2 was first synthesized, followed by Au deposition under a 350 W Xe lamp light source [82]. The synthesized Au/meso-TiO_2 exhibited the characteristic features of mesocrystal structures, including a substantial surface area of 211.3 m^2/g and high crystallinity.

Other efficient synthesis techniques, such as (atomic layer deposition) ALD, ball milling, microwave-assisted, and impregnation methods, are widely used for photocatalysts but rarely for dual-functional ones, highlighting opportunities for further research [83–86].

4. Hydrogen production and pollutant degradation *via* photocatalysis

4.1. Hydrogen production

Modern society heavily depends on fossil energy, and H_2 production techniques, such as methanol/methane steam reforming, natural gas reforming, and water splitting, have been extensively studied [87]. Among these, photocatalytic overall water splitting (OWS), which decomposes water into H_2 and O_2, is considered an ideal method for H_2 production (Eq. 1).

$$H_2O \rightarrow H_2 + 1/2O_2,\ \Delta G = 237\ \text{kJ/mol} \quad (1)$$

For suitable photocatalytic semiconductors, the conduction band minimum (CB) should be more negative than the redox potential of H^+/H_2. The maximum of the valence band (VB) should be more positive than the redox potential of O_2/H_2O [88].

Besides the thermodynamic, photocatalysts with narrow band gaps to maximize solar light absorption and appropriate band positions are essential prerequisites for effective photocatalytic water splitting [89]. However, narrow band gaps hinder photogenerated charge separation, and rapid recombination (ps-μs) further limits efficiency; effective photocatalytic H_2 evolution relies on light absorption, charge separation/transport, and surface catalytic reactions [90]. For the photocatalytic OWS, the generated H_2 and O_2 gases should be observed in a stoichiometric ratio of 2:1, as per the balanced chemical equation. The OWS reaction can be separated into two half-reactions (Eqs. 2 and 3):

$$2H^+ + 2e^- \rightarrow H_2\ (\text{HER}) \quad (2)$$

$$H_2O + 2h^+ \rightarrow 1/2O_2\ (\text{OER}) \quad (3)$$

Due to the high energy barrier of overall water splitting (OWS), sacrificial agents are often used to study half-reactions, which are thermodynamically more feasible (ΔG < 237 kJ/mol, often negative). Researchers increasingly use biomass oxidation as a hole-scavenging strategy, enabling simultaneous H_2 production and value-added chemical synthesis. Moreover, Li *et al.* prepared Pd-loaded CdS photocatalysts for water splitting, with CdS-Pd (3.83 ‰) achieving H_2 evolution rates of 947.93 μmol g^{-1} h^{-1} without and

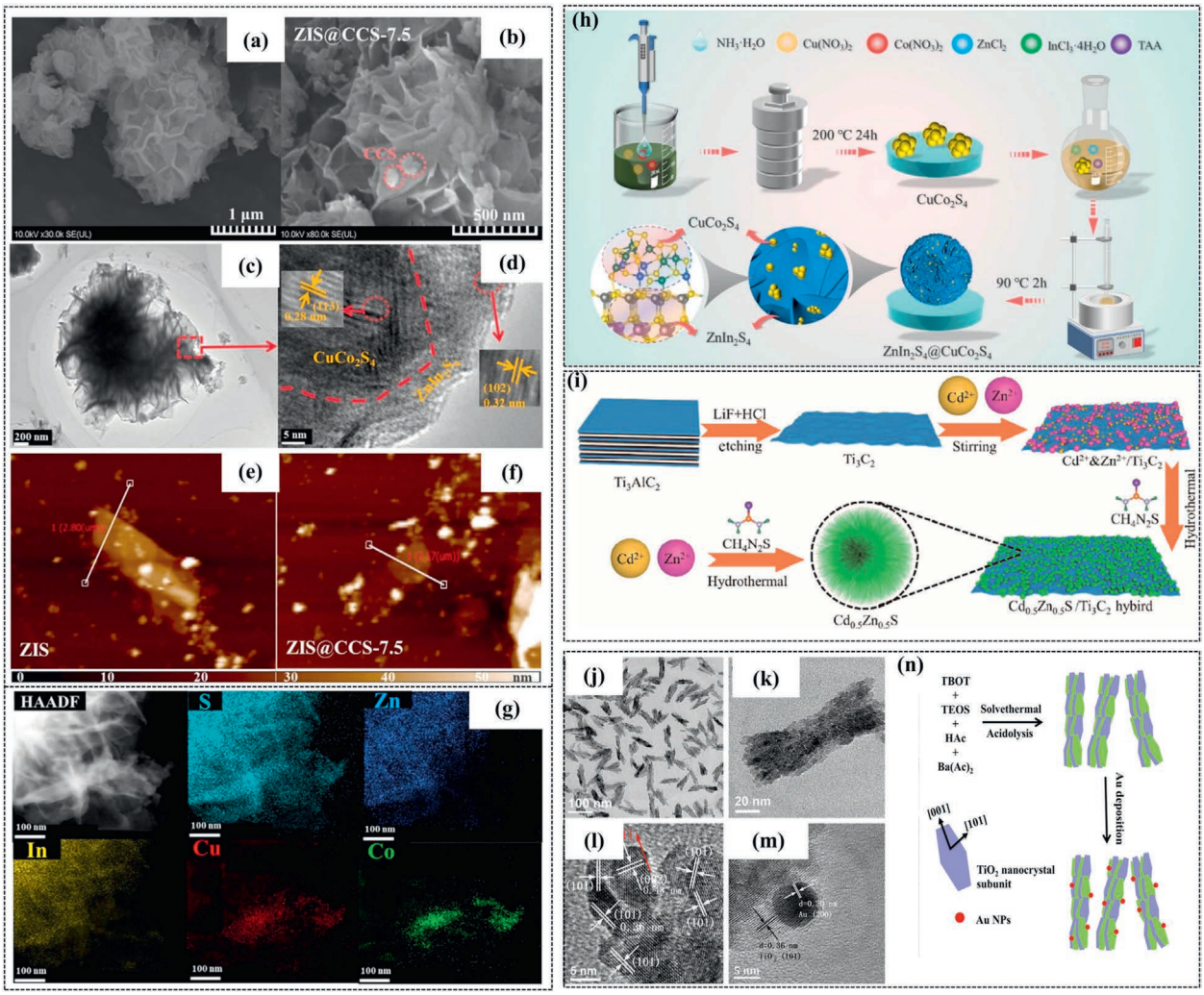


Fig. 5. SEM images of (a) ZIS and (b) ZIS@CCS-7.5. (c) TEM images of ZIS@CCS-7.5. (d) High-resolution transmission electron microscopy (HRTEM) image of ZIS@CCS-7.5. AFM images of (e) ZIS and (f) ZIS@CCS-7.5. (g) High-magnification TEM-EDS mappings of ZIS@CCS-7.5. (h, i) Synthesis diagram of ZIS@CCS and 0D $Cd_{0.5}Zn_{0.5}S$/2D Ti_3C_2, respectively. Reprinted with permission [21,80]. Copyright 2022, 2023. Elsevier. (j, k) TEM images of meso-TiO_2. (l, m) HRTEM images of meso-TiO_2 and ^{1}Au/meso-TiO_2 composite, respectively. (n) Schematic illustration of the formation process of the Au/meso-TiO_2 composites. Reprinted with permission [82]. Copyright 2020, Elsevier.

7335.85 μmol g^{-1} h^{-1} with sacrificial agents (Figs. 6a-c) [91]. As shown in Figs. 6d-f, photocatalysts maintained good stability after four months of cycling. As illustrated in Fig. 6g, a large number of bubbles appeared under outdoor sunlight irradiation, which provided the visual evidence to demonstrate the high efficiency of CdS-Pd (3.83 ‰). The water splitting process was demonstrated to be the rate-controlling step of HER *via* DFT calculation and XPS spectra (Fig. 6h), and CdS-Pd displayed a smaller activation barrier (0.93 eV) than pure CdS (1.31 eV). Besides noble metals, transition metal atoms offer significant advantages by reducing the reliance on noble metals and overcoming the activity limitations associated with noble metal atoms. For example, Wang *et al.* synthesized Co-O-Pt dimers on TiO_2, which outperformed single-atom Pt catalysts in H_2 evolution by altering the electronic structures of Pt and Co for improved metal utilization [92].

Compared to metal oxide/sulfide, MOFs and g-C_3N_4 have a higher specific surface area, which is capable of providing more active sites during catalysis. Zhuang *et al.* synthesized lignin-derived carbon and further anchored Pt single atoms *via* Pt-N_4 coordination effect to synthesize Pt-NLCDs (nitrogen-doped liquid crystal devices) photocatalysts [93]. The stable Pt-N_4 structure benefited the charge accumulation on the Pt single atoms. Based on the simulation results (Figs. 6i and j), only pyridinic N could form Pt-N_4 coordination structure, and such a structure is equipped with $\pi \rightarrow \pi^*$ and $n \rightarrow \pi^*$ electron transitions, which make it an ideal cocatalyst for photocatalytic H_2 evolution. In addition, the partial density of states (DOS) of Pt-NLCDs was also recorded to demonstrate that the p electrons of nitrogen contribute most. This coordination structure enables the loaded Pt single atoms to accumulate more negatively polarized charges, effectively shifting their d-band centers closer to the Fermi level. This shift enhances the dissociation of H_2. By further combining CdS and Pt-NLCDs (Pt-NLCDs@CdS), the heterojunction effect was enhanced, thus benefiting the transportation of photogenerated electrons. Finally, Pt-NLCDs@CdS reached hydrogen evolution rates of 46.10 mmol h^{-1} g^{-1}. Guo *et al.* developed a novel catalyst composed of a CdS/Ni-MOF composite with an optimal CdS loading of 40 wt%, which demonstrated an impressive hydrogen production rate of 2508 μmol g^{-1} h^{-1} under visible light [94]. This rate was approximately eight times greater than that of pure CdS. Ni-MOF acted as an efficient platform for the rapid transfer of photogenerated electrons, resulting in enhanced photocatalytic performance. And wildly speared Ni^{2+} catalystic sites also benefited the hydrogen evolution.

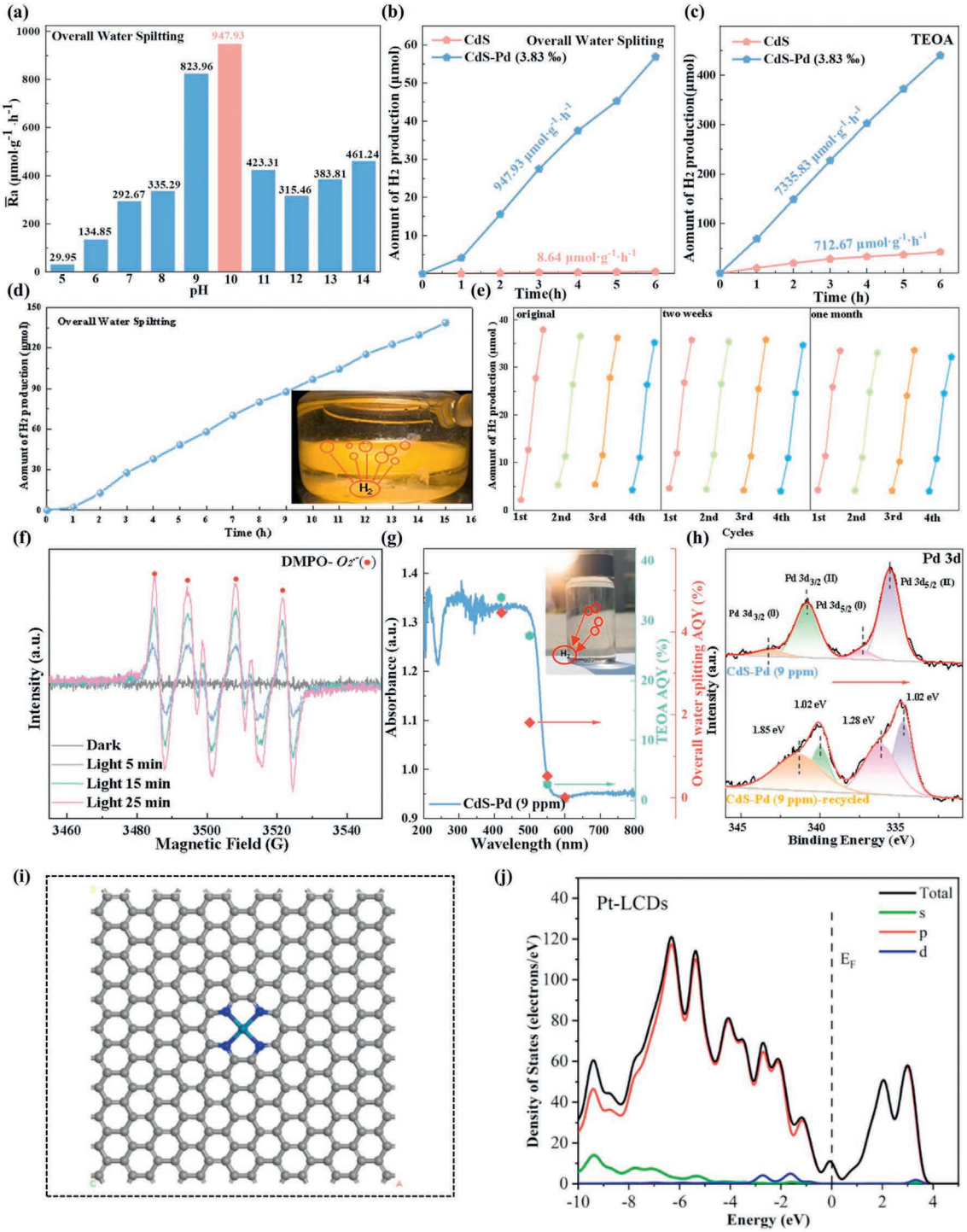


Fig. 6. (a) HER performances under different pH values. (b, c) HER rates of CdS and CdS (3.83 ‰) with the absence or presence of sacrificial agents, respectively. (d, e) Sample durability. (f) Electron paramagnetic resonance (EPR) spectra of CdS-Pd (3.83 ‰) aqueous dispersion during different illuminated time (0, 5, 15, and 25 min). (g) H_2 evolution under sunlight. (h) Pd 3d XPS spectra of fresh and recycled CdS-Pd (3.83 ‰). Reprinted with permission [91]. Copyright 2021, Elsevier. (i, j) Optimized Pt-NLCDs structure (top view), and partial density of states of Pt-NLCDs. Reprinted with permission [93]. Copyright 2022, Elsevier.

4.2. Pollutant degradation

In printing and dyeing wastewater, inorganic heavy metal ions, organic dyes, and antibiotic wastewater threaten human health and the natural environment [10]. Textile wastewater commonly contains heavy metals (Cr, Pb, Cd, Zn) and synthetic dyes (*e.g.*, RhB, methyl blue). These contaminants pose serious risks through bioaccumulation and toxicity, including neurological and renal disorders, carcinogenicity, and ecological disruption, largely due to untreated industrial effluent discharge [8,95]. Apart from printing and dyeing pollutants, residues of pharmaceuticals and personal care products (PPCPs) gradually become another threat in the aquatic ecosystem [96–98]. As summarized in Fig. 7, light excitation generates electron-hole pairs on the photocatalyst, where electrons form $^{\bullet}O_2^-$ and H_2O_2, and holes oxidize H_2O and $^{\bullet}O_2^-$ to produce $^{\bullet}OH$ and other reactive species.

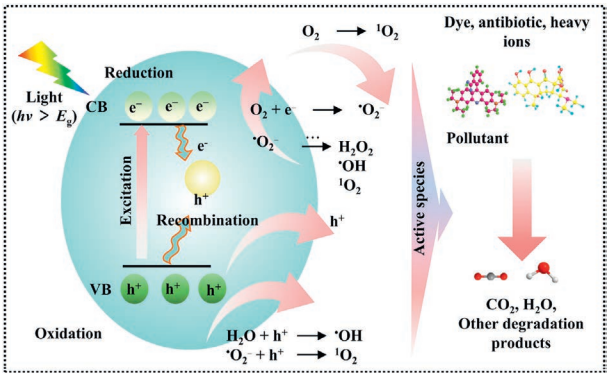


Fig. 7. Schematic illustration of photocatalytic degradation mechanism.

Recent research has focused on various methods for removing these contaminants from wastewater. Photocatalysis has emerged as a powerful tool for environmental remediation, demonstrating exceptional efficacy in the photocatalytic degradation of organic and inorganic pollutants. Shangguan *et al.* developed a $CuFeS_2$ co-decorating with Ag(I) and Ag(0) 3.63 wt% loading content for synergistic Cr(VI) and RhB removal [10]. As shown in Fig. S2a (Supporting information), the band gap decreased by 1.21 V at most with Ag loading. Therefore, Ag(0) and Ag(I) single atoms could effectively separate photon-generated carriers, which resulted in the enhanced effect of Cr(VI) and RhB degradation. Besides, a large specific surface area provides more active sites for pollutant adsorption. However, loading the content of single atoms benefits the effect of degradation in a certain range. Xu *et al.* developed an atomically Pt-anchoring nanoporous TiO_2 film with exposed [001] facets [99]. As illustrated in Figs. S2b-e (Supporting information), TiO_2 with 0.1 wt% Pt loading degraded most ethenzamide and reached the highest apparent rate constant (0.108 min^{-1}), and ethenzamide was degraded within 15 min. Pt single atoms acted as electron centers in {001}, which optimized the conversion of surface hydroxyl groups to hydroxyl radical groups. Moreover, molecular oxygen was combined with generated photoelectrons in {101} facets, which resulted in the creation of $^{\bullet}O_2^-$. The enriched heteroatoms (such as N, O, S, B) coordination environment could generate new functional electronic states and active sites, and thus change the mechanism of catalytic reactions. Wang *et al.* fabricated the single-metal-atom-oxides-based (WO_3) photocatalyst, which demonstrated a new mechanism of single-site catalysis called *quasi*-atom physics [100]. An electron in the spin-up orbital was excited and thus promoted to the lowest occupied molecular orbital +1 state, which resulted in the generation of the photogenerated electrons. Due to such a mechanism, single-tungsten-atom-oxide (STAO) resulted in a 0.24 s^{-1} degradation rate and 64.82 % of apparent quantum yield (AQY) of dyes. Besides a certain electron structure, combining specific microstructure with defect engineering of support could result in the modification of the degradation of the pollutant. Zhang *et al.* introduced N vacancy to tubular porous g-C_3N_4 (Nv-TCN) with atomically dispersed Mo (Mo/Nv-TCN) *via* gas etching [101]. The large specific surface area of the tubular morphology helped to prevent the cluster of Mo atoms, while the nitrogen defect facilitated the formation of a stable Mo-2C/2N configuration between the light absorbers and the Mo sites. Introduced N with exposed lone pairs of electrons could form hydrogen bonds with H-containing groups in TC. And Mo single atoms might have surface complexation with the polar functional groups of TC molecules. All these interactions optimized the adsorption effect of Mo/Nv-TCN. As shown in Figs. S2f-i (Supporting information), while 10-Mo/Nv-TCN with Mo loading content 1.21 wt% had the highest degradation efficiency, the Mo content in 10-8Mo/Nv-TCN was not the highest, which was similar to other studies. Furthermore, the degradation pathway of TC was detected by mass spectrum (Fig. S2j in Supporting information). TC was converted into CO_2, H_2O, or other small molecules after hydroxylation, dehydroxylation, ring-opening, deamination reaction, and mineralization reactions. As shown in Figs. S2k-o (Supporting information), compared with TCN, the N vacancy impaired the conjugation structure of the triazine ring, which broke the delocalized π bond, thus resulting in the uneven distribution of charge.

4.3. Pollutant degradation simultaneous with hydrogen evolution

Over the past decades, converting waste, such as wastewater, waste gases, and cellulose, into hydrogen has been explored, enabling simultaneous photocatalytic H_2 evolution and pollutant degradation, as shown in Fig. S3a (Supporting information) [102].

4.3.1. Photocatalytic hydrogen evolution simultaneously with pollutant degradation

In the early 2000s, Li *et al.* were one of the first groups to investigate the hydrogen evolution simultaneously with pollutant degradation on TiO_2/Pt [103]. Oxalic acid, formic acid, and formaldehyde were used as electron donors under UV irradiation, respectively. Through *in situ* attenuated total reflection infrared spectroscopy (ATRIR), the authors suggested that the photocatalytic performance of different electron donor systems could be related to the nature of the interaction between the electron donor and the surface site of TiO_2. The strong adsorption of electron donors on TiO_2 was conducive to electron transfer and H_2 evolution.

At present, it is difficult for H_2 production to occur simultaneously with pollutant degradation in one system since the pollutant degradation is usually an aerobic process, whereas hydrogen evolution is an anoxic one. During the process of pollutant degradation, $^{\bullet}O_2^-$ is required, which is generated from the reaction between O_2 and photo-generated electrons (e^-). On the contrary, O_2 is not preferable for hydrogen evolution since O_2 is capable of oxidizing H_2 to H_2O. Even so, researchers have strived to combine these two purposes in one single system to achieve dual-functional photocatalysis [104]. There are two ways for pollutant degradation, simultaneous with hydrogen evolution. One is the $^{\bullet}O_2^-$-mediated way, another is the non-$^{\bullet}O_2^-$-mediated way [105]. The former requires $^{\bullet}O_2^-$ generating from O_2 for pollutant degradation, which consumes electrons and thus weakens the activity of hydrogen evolution. And $^{\bullet}O_2^-$ generation should satisfy the thermodynamic requirements (−0.046 eV *vs.* normal hydrogen electrode (NHE), pH 0). The latter requires holes (h^+) in the valence band of a semiconductor reacting with H_2O to generate $^{\bullet}OH$ or pollutant degradation, which requires the VB position to be more positive than 2.38 eV (*vs.* NHE, pH 0). In this pathway, electrons for hydrogen evolution proceeds well but pollutant degradation is hindered [105]. This is mainly due to the active species in pollutant degradation being demonstrated to be $^{\bullet}O_2^-$ instead of $^{\bullet}OH$ [103].

For simultaneous H_2 production and pollutant degradation, pollutants must act as electron donors to enhance photogenerated electron transfer and suppress electron-hole recombination. Moreover, the oxidative degradation of organic pollutants can be carried out at the same time as the hydrogen reduction of water, which can realize the coordination of pollutant removal and hydrogen evolution. It is advantageous to generate electrons during the pollutant oxidation process, as these electrons can be utilized for the reduction of protons or H_2O. On the contrary, the photocatalytic degradation of some pollutants is difficult to cooperate with hydrogen evolution because it is difficult to be fully mineralized [20]. In addition, the redox potential of some organic pollutants can not match the energy band position of the photocatalysts, which is not

conducive to electron transfer and makes it difficult to achieve simultaneous hydrogen production. Besides, irradiation intensity can enhance the degradation rate of organic pollutants but may compromise H_2 evolution efficiency [106]. The solution pH affects surface charge and band-edge positions, influencing both pollutant oxidation and proton reduction processes [107]. Additionally, the type of sacrificial agent governs the competition between organic oxidation and hydrogen generation, thereby modulating the overall dual functionality [108].

Regarding the origin of hydrogen, some researchers have suggested that it is derived from H_2O or protons, while pollutants are ultimately mineralized or decomposed into CO_2 and H_2O. Jiang *et al.* used quantum-dot-modified g-C_3N_4 catalysts for *p*-chlorophenol (4-NP), bisphenol A (BPA), and TC photocatalytic degradation simultaneously with hydrogen evolution (Fig. S3b in Supporting information) [109]. Their group employed liquid chromatography mass spectrometry (LC-MS) to investigate the reason for the different photocatalytic rate of hydrogen production in the presence of different organic pollutants. As shown in Figs. S3c and d (Supporting information), no hydrogen was generated during the degradation of organic pollutants, which proved that the hydrogen was evolved from water splitting instead of the decomposition of organic pollutants. Moreover, the consumption of electrons by 4-NP hindered the rate of hydrogen evolution, indicating that the hydrogen evolution rates are influenced by the types of pollutants present. Liu *et al.* reported similar results [110]. As shown in Fig. S3e (Supporting information), the $ZnIn_2S_4$-based 3-D nitrogen-doped carbon cage (NGC) encapsulated ultrasmall MoC nanoparticles (MoC@NGC/ZIS) were used for RhB degradation simultaneously with hydrogen evolution. The photogenerated electrons were transferred from ZIS to MoC *via* NGC, and reduced protons or H_2O to H_2. And the paired holes at the VB of the ZIS degraded RhB into small molecules. In general, hydrogen originates from the reduction of H_2O or protons by photogenerated electrons. Therefore, it is essential to design specific structures of photocatalysts that enhance the efficient separation of photoexcited electron-hole pairs, enabling the simultaneous degradation of pollutants and the production of photocatalytic H_2.

Cho synthesized TiO_2 modified with graphene oxide (GO) along with Pt and fluoride (F) for 4-chlorophenol (4-CP) degradation simultaneously with HER [105]. As shown in Fig. 8a, prepared samples showed about 20 μmol H_2 evolution in 7 h and approximately 80 % 4-CP degradation. Both Pt/GO/TiO_2-F and Pt/TiO_2-F demonstrated significantly enhanced hydrogen production compared to Pt/GO/TiO_2 and Pt/TiO_2, respectively, while the H_2 production from TiO_2 and F-TiO_2 was minimal. Notably, Pt/GO/TiO_2-F exhibited superior activity compared to both Pt/TiO_2-F and Pt/GO/TiO_2. This indicates that the ternary hybrid components (Pt, GO, and F) work synergistically to significantly enhance hydrogen production. Similarly, the degradation rates were highly enhanced only with Pt/GO/TiO_2-F and Pt/TiO_2-F and limited or insignificant with other catalysts (Fig. 8b). As a result, the coexistence of Pt and F is crucial for achieving dual photocatalytic activity, while the incorporation of graphene oxide as a third component further enhances this activity. As illustrated in Figs. 8c-f, TiO_2 was used to generate electrons and holes, GO and Pt were introduced to conduct electrons, surface fluorination replaced the surface hydroxyl groups, which reduces the hole-trapping efficiency. As a result, the trapped electrons in Pt had a longer lifespan, allowing them to preferentially react with protons and water rather than with surface-trapped holes, which facilitated the simultaneous production of hydrogen and the degradation of organic substrates.

He *et al.* synthesized Bi single atoms modified on $ZnIn_2S_4$, achieving hydrogen production rates of up to 3658.8 μmol g^{-1} h^{-1} and $PhCH_2OH$ degradation rates of 1030.4 μmol g^{-1} h^{-1} [111]. The introduced Bi formed the Schottky junction with $ZnIn_2S_4$ (ZBIS-1); electrons were transferred from the conductive band of $ZnIn_2S_4$ to the atomically dispersed Bi, resulting in the formation of holes in the valence band of $ZnIn_2S_4$. And covalent Bi-S coordination bonds in ZBIS-1 improved charge mobility and thus enhanced photocatalytic activity, which was demonstrated by DFT calculation (Fig. 8g). As shown in Fig. 8h, EPR revealed that the groups centered on carbon-free radicals were generated under the light irradiation, which indicated that the degradation process of $PhCH_2OH$ was indeed triggered by the photocatalyst driven by visible light. Moreover, they extended to different aromatic alcohols and found that the electronegativity of the R group in R-$PhCH_2OH$ (R = Me, OH, Cl) would affect the catalytic activity (Fig. 8i).

4.3.2. Photocatalytic hydrogen evolution simultaneously with organic conversion to value-added products

In the late 1970s and 1980s, experiments were initiated to utilize organic substrates for photocatalytic dehydrogenation. During this period, the conversion of carbohydrates into hydrogen gas was investigated, a process commonly referred to as photoreforming. Similar to dual-functional photocatalysis, photoreforming refers to the hydrogen evolution from organic compounds. Recently, research has increasingly focused on transforming dehydrogenated organic substrates into value-added organic products, such as benzylamine [22], benzaldehyde [80], aldehydes [6], and other compounds.

As shown in Fig. 8j, She *et al.* synthesized a sandwich-like Pd@TiO_2@$ZnIn_2S_4$ nanobox *via* the wet chemical method, which exhibited a superior hydrogen evolution rate of 5.35 mmol g^{-1} h^{-1} and a benzylamine (BA) conversion rate (>99 %) [22]. Compared to the commonly used sacrificial agents, H_2 evolution rates achieved the highest (Figs. 8k-n). As shown in Fig. 8o, upon exposure to simulated solar light, both hollow TiO_2 and $ZnIn_2S_4$ were activated, generating electrons and holes. The conduction band was positioned higher than that of TiO_2, while its valence band was lower. This allowed electrons to transfer from the CB of $ZnIn_2S_4$ to that of TiO_2, with holes being collected at the VB of $ZnIn_2S_4$. The electrons were then utilized to reduce H_2O and protons for hydrogen production, and the holes facilitate the oxidation of benzyl alcohol (BA). Tao *et al.* synthesized Ti_3C_2 nanosheets decorated with $Cd_{0.5}Zn_{0.5}S$ nano-spheres, resulting in the formation of the Schottky barrier [80]. The increased number of Schottky barrier sites resulting from a larger contact area can effectively inhibit the recombination of photogenerated electrons and h^+. Notably, it simultaneously achieved a hydrogen evolution rate of 5.3 mmol g^{-1} h^{-1} and a benzaldehyde generation rate of 29.3 mmol g^{-1} h^{-1} when benzyl alcohol was employed as a sacrificial agent. These rates were approximately 3.2 times and 2.0 times higher, respectively, than those of pristine $Cd_{0.5}Zn_{0.5}S$. For pristine $Cd_{0.5}Zn_{0.5}S$, the photoinduced electrons generated from the VB could jump to the CB and then combine with the protons in H_2O to produce H_2, the H_2 originated from the H_2O and protons. Moreover, Liu and his co-workers were one of the first researchers to study the simultaneous production of H_2 and valuable organic chemicals *via* MOF-based material (Pt/PCN-777) [112]. Their group used benzylamine as the sacrificial agent for proton reduction, which avoided water oxidation reaction and achieved a hydrogen evolution rate of 332 μmol g^{-1} h^{-1}.

4.3.3. Hydrogen evolution simultaneously with wastewater splitting in real life

Achieving complete mineralization of organic pollutants during tertiary wastewater treatment *via* photocatalytic oxidation can be challenging. This difficulty arises because, during the process, several heavier organic molecules (in terms of molecular weight) are converted into smaller intermediate molecules rather than being fully transformed into CO_2 and H_2O. However, these intermediate organic products are better suited for use as electron donors in

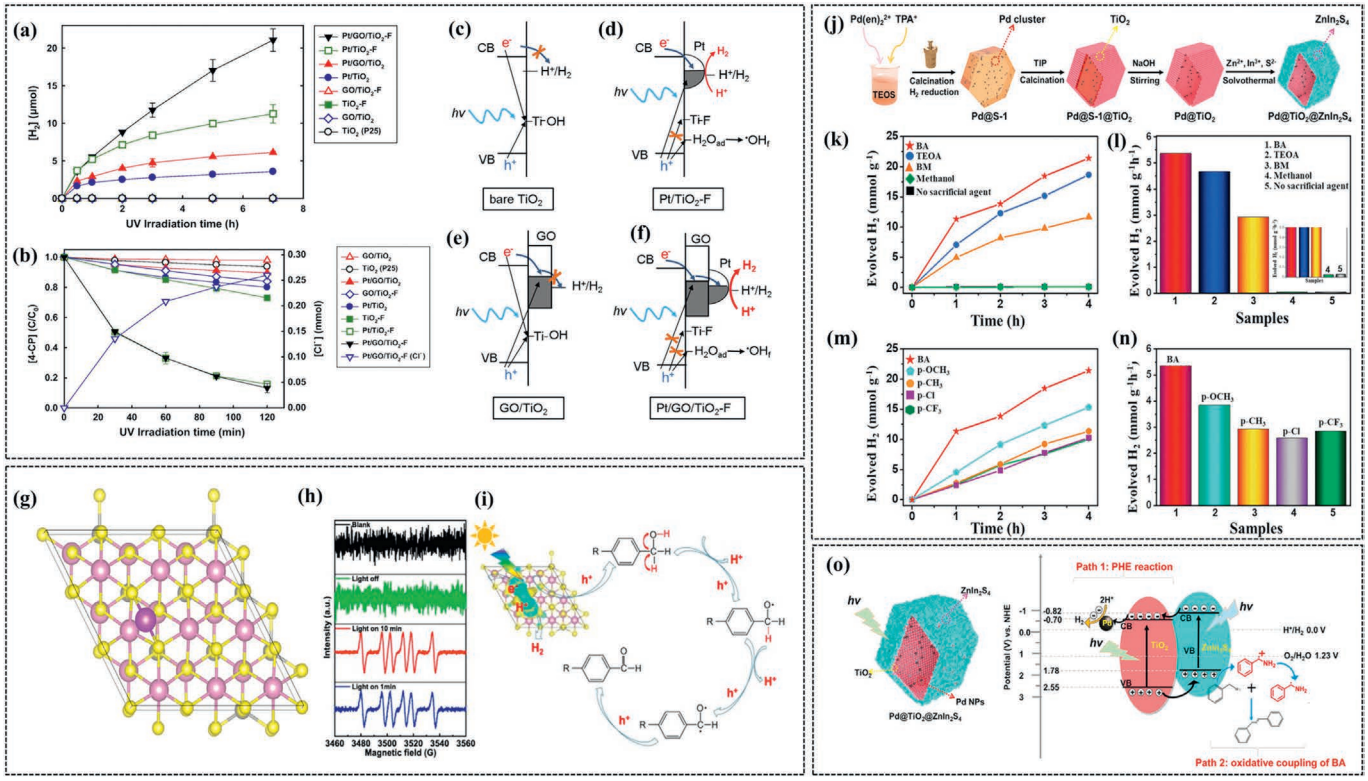


Fig. 8. (a) Time profiles of H_2 production in the irradiated suspension of hybrid photocatalysts with 4-CP and (b) concurrent degradation of 4-CP. Schematic illustrations of interfacial charge transfer and recombination occurring on (c) bare TiO_2, (d) Pt/TiO_2-F, (e) GO/TiO_2, and (f) Pt/GO/TiO_2-F in the absence of O_2. Reprinted with permission [105]. Copyright 2015, Elsevier. (g) DFT calculation of Bi-S coordination bonds in ZBIS-1. (h) EPR detection of *in-situ* formed carbon-centered radicals under different reaction conditions. (i) Mechanism of benzyl alcohol oxidation into benzaldehyde. Reprinted with permission [111]. Copyright 2023, Elsevier. (j) Preparation method of Pd@TiO_2@$ZnIn_2S_4$. (k) Time courses curves and (l) bar chart of PHE of Pd@TiO_2@$ZnIn_2S_4$ with various SEDs. (m) Time courses curves and (n) bar chart of dual-functional photocatalytic reactions for cooperative PHE and oxidation coupling of BA with different substituents. (o) Schematic illustration of the dual-functional photocatalytic mechanism for hydrogen evolution simutanously with BA oxidation over Pd@TiO_2@$ZnIn_2S_4$. Reprinted with permission [22]. Copyright 2021, Elsevier.

photocatalytic H_2 evolution [113]. Moreover, pollutants can hardly be degraded under anoxic conditions. Based on these, Huang *et al.* reported a cascading oxic-anoxic photocatalytic process to produce H_2 from natural organic matter (human acid (HA)) [114]. As shown in Fig. S4 (Supporting information), this technique concluded two processes: Photocatalytic oxic pre-treatment of organic matter and photocatalytic hydrogen production under anoxic conditions. Moreover, oxygen-containing intermediates served as electron donors. The use of a dual-functional photocatalyst to recover energy from wastewater is not only a sustainable approach but also has the potential to reduce the overall costs of wastewater treatment. While significant progress has been made in visualizing the practical applications of this field through extensive research efforts in recent years, there remain several challenging issues to address, particularly concerning the photocatalytic activity of the materials. For example, there are very few studies that exhibit a high rate of H_2 evolution. Therefore, future research should focus on developing efficient and durable dual-functional photocatalysts, exhibiting wide light absorption and low charge carrier recombination rates.

5. Future perspective

For hydrogen evolution, it is essential to identify the sources of hydrogen first. Although the antibiotic serves as a sacrificial reagent, in most studies, hydrogen is generated from an H_2O splitting reaction, which requires a high energy. Therefore, it is critical to utilize the hydrogen generated from the oxidation of pollutants. Furthermore, it is crucial to determine whether the antibiotics contribute to this process, as this insight is vital for understanding the conversion of waste to energy. Secondly, the experiments are consistently conducted under anaerobic conditions, which benefits the hydrogen production. However, pollutants can hardly be degraded in an anaerobic environment. So it is necessary to investigate the byproducts under aerobic conditions.

For pollutant degradation and conversion of value-added products, different pollutants and organic compounds exhibit varying oxidation potentials. Therefore, the position of the VB in photocatalysts is crucial as it determines whether the h^+ can directly oxidize pollutants. Additionally, it is important to examine whether the reaction sites of these pollutants attacked by active sites follow any universal patterns. Moreover, the products generated by oxidation through $^{\bullet}OH$ and h^+ may differ, and these differences need to be further explored.

For the implementation of dual-functional photocatalysis in real life, the development of efficient and stable photocatalysts is the key to realizing the practical application of photocatalysis technology. Moreover, most semiconductor photocatalysts have a low utilization rate of visible light, which limits their practical application. The high cost of photocatalytic hydrogen production technology limits its large-scale application. It is both logical and energy-efficient for H_2 production to utilize hydrogen sources derived from pollutants or organic matter.

Moreover, improving photocatalytic efficiency requires understanding the kinetics and thermodynamics of charge separation, transfer, and surface reaction dynamics, providing a theoretical basis for catalyst design and reaction optimization. In addition, despite the significant progress in synergistic dual-functional photocatalysis, several challenges remain to be addressed before practical application. First, the scalability of material synthesis is

limited, as many current methods rely on complex procedures or costly precursors. Second, long-term stability under real operating conditions, particularly in the presence of competing ions or fluctuating light intensities, requires further investigation. Finally, overcoming the intertwined challenges of scalable synthesis, operational stability, and economic feasibility will be pivotal for advancing dual-functional photocatalysis from laboratory studies to sustainable industrial applications.

6. Conclusion

In this mini-review, recent advances in dual-functional photocatalysts for simultaneous hydrogen evolution and pollutant degradation were summarized. Widely studied materials include metal oxides/sulfides, MOFs, and g-C_3N_4. Common strategies to enhance photocatalytic activity involve metal and nonmetal modification, sensitization, morphology engineering, p-n heterojunction formation, and the use of co-catalysts. Efficient photocatalysis relies on the simultaneous utilization of holes and electrons for pollutant degradation and hydrogen production under suitable irradiation conditions. This requires an appropriate band structure that enables effective charge transfer, as well as strategies to improve electron-hole separation and suppress recombination, thereby enhancing photocatalyst reactivity.

CRediT authorship contribution statement

Hao Bi: Writing – original draft, Visualization, Formal analysis. **Guang Yang:** Conceptualization. **Qian Liu:** Conceptualization. **Ran Zhao:** Conceptualization. **Fangyuan Chen:** Writing – review & editing, Supervision, Funding acquisition. **Zhurui Shen:** Investigation, Funding acquisition, Conceptualization.

Declaration of competing interest

The authors declare that they have no known competing financial interests or personal relationships that could have appeared to influence the work reported in this paper.

Acknowledgments

This work was financially supported by the National Key Research and Development Program of China (No. 2023YFC3708005), the National Natural Science Foundation of China (Nos. 22172080 and 22406004), the Fundamental Research Funds for the Central Universities, Nankai University (No. 63243114).

Supplementary materials

Supplementary material associated with this article can be found, in the online version, at doi:10.1016/j.cclet.2026.112463.

References

[1] F. Shao, X. Zhang, X. Sun, et al., J. Dispers. Sci. Technol. 42 (2021) 1274–1285.
[2] B. Zhou, Q. Gao, H. Wang, et al., J. Air Waste Manage. Assoc. 62 (2012) 1394–1402.
[3] Y. Cao, S. Chen, Q. Luo, et al., Angew. Chem. Int. Ed. 56 (2017) 12191–12196.
[4] A. Chatzitakis, C. Berberidou, I. Paspaltsis, et al., Water. Res. 42 (2008) 386–394.
[5] D. Wang, R. Huang, W. Liu, et al., ACS Catal. 4 (2014) 4254–4260.
[6] G. Han, Y. Jin, R. Burgess, et al., J. Am. Chem. Soc. 139 (2017) 15584–15587.
[7] Y. Yang, Z. Yan, S. Yang, et al., J. Clean. Prod. 377 (2022) 134397.
[8] R. Trofimovaite, C. Parlett, S. Kumar, et al., Appl. Catal. B 232 (2018) 501–511.
[9] W. Mao, L. Zhang, Y. Liu, et al., Chemosphere 263 (2021) 127988.
[10] Y. Shangguan, Y. Zhou, R. Zheng, et al., Chin. Chem. Lett. 32 (2021) 3450–3456.
[11] J. Liu, H. Li, J. Zhang, et al., J. Colloid. Interface Sci. 628 (2022) 637–648.
[12] F. Wang, Y. Wang, Y. Feng, et al., Appl. Catal. B: Environ. 221 (2018) 510–520.
[13] A. Rezaee, G. Pourtagi, H. Hossini, et al., J. Appl. Polym. Sci. 133 (2015) 43051.
[14] N. Stock, J. Peller, K. Vinodgopal, et al., Env. Sci. Technol. 34 (2000) 1747–1750.
[15] Z. Wang, C. Li, K. Domen, Chem. Soc. Rev. 48 (2019) 2109–2125.
[16] J. Xing, J. Chen, Y. Li, et al., Chem. Eur. J 20 (2014) 2138–2144.
[17] N. Cheng, S. Stambula, D. Wang, et al., Nat. Commun. 7 (2016) 13638.
[18] S. Kampouri, T.N. Nguyen, M. Spodaryk, et al., Adv. Funct. Mater. 28 (2018) 1806368.
[19] G. Zhou, M. Wu, Q. Xing, et al., Appl. Catal. B 220 (2018) 607–614.
[20] Z. Wei, J. Liu, W. Shangguan, Chin. J. Catal. 41 (2020) 1440–1450.
[21] R. Wang, W. Yu, N. Fang, et al., Appl. Catal. B: Environ. 341 (2024) 123284.
[22] P. She, J. Qin, J. Sheng, et al., Small 18 (2022) 2105114.
[23] J. Wang, S. Yin, Q. Zhang, et al., J. Catal. 404 (2021) 89–95.
[24] J. Luo, S. Zhang, M. Sun, et al., ACS Nano 13 (2019) 9811–9840.
[25] C. Gao, S. Chen, Y. Wang, et al., Adv. Mater. 30 (2018) e1704624.
[26] P. Suja, J. John, T. Rajan, et al., J. Mater. Chem. A 11 (2023) 8599–8646.
[27] C. Gao, J. Low, R. Long, et al., Chem. Rev. 120 (2020) 12175–12216.
[28] W.K. Darkwah, K.A. Oswald, Nanoscale Res. Lett. 14 (2019) 234.
[29] Z. Zhou, Y. Zhang, Y. Shen, et al., Chem. Soc. Rev. 47 (2018) 2298–2321.
[30] M. Mubeen, K. Deshmukh, D. Peshwe, et al., Spectrochim. Acta A 207 (2019) 301–306.
[31] W. Zhang, D. Xu, F. Wang, et al., Nanoscale Adv. 3 (2021) 4370–4387.
[32] Y. Lu, W. Wang, H. Cheng, et al., Int. J. Hydrog. Energy 47 (2022) 3733–3740.
[33] W. Zhang, J. Yin, C. Chen, et al., Chem. Eng. Sci. 241 (2021) 116709.
[34] L. Cong, H. Mu, S. Zhang, et al., Nano 12 (2017) 37–46.
[35] Q. Liang, Z. Li, Y. Bai, et al., Small 13 (2017) 1603182.
[36] Z. Wei, J. Liu, W. Fang, et al., Chem. Eng. J. 358 (2019) 944–954.
[37] H. Dou, Y. Qin, F. Pan, et al., Catal. Sci. Technol. 9 (2019) 4898–4908.
[38] H. Feng, H. Li, X. Liu, et al., Chem. Eng. J. 428 (2022) 132045.
[39] L. Jiao, H. Jiang, Chem 5 (2019) 786–804.
[40] Q. Zuo, T. Liu, C. Chen, et al., Angew. Chem. Int. Ed 58 (2019) 10198–10203.
[41] J. Wu, H. Zhou, Q. Li, et al., Adv. Energy Mater. 9 (2019) 1900149.
[42] H. Haroon, Q. Xiang, Small 20 (2024) 2401389.
[43] E. NyelaMusa, K. Stylianou, Mol. Syst. Des. Eng. 8 (2023) 151–166.
[44] R. Abazari, S. Sanati, N. Li, et al., Inorg. Chem. 62 (2023) 18680–18688.
[45] S. Kampouri, C. Ireland, B. Valizadeh, et al., ACS Appl. Energy Mater. 1 (2018) 6541–6548.
[46] X. Ge, P. Zhou, Q. Zhang, et al., Angew. Chem. Int. Ed 59 (2020) 232–236.
[47] P. Zhou, Q. Zhang, Y. Chao, et al., Chem 7 (2021) 1033–1049.
[48] P. Zhou, Q. Zhang, Z. Xu, et al., Adv. Mater. 32 (2020) e1904249.
[49] X.F. Zheng, J.L. Xia, Z.Y. Nie, et al., Chem. Eng. J. 442 (2022) 136350.
[50] X. Shi, C. Dai, X. Wang, et al., Nat. Commun. 13 (2022) 1287.
[51] T. He, S. Chen, B. Ni, et al., Angew. Chem. Int. Ed. 57 (2018) 3493–3498.
[52] H. Dong, G. Zeng, L. Tang, et al., Water. Res. 79 (2015) 128–146.
[53] W. Teoh, J. Scott, R. Amal, J. Phys. Chem. Lett. 3 (2012) 629–639.
[54] Z. Hu, X. Wang, H. Dong, et al., J. Hazard. Mater. 340 (2017) 1–15.
[55] S. Zhang, B. Bai, J. Liu, et al., Catalysts 11 (2021) 1168.
[56] Y. Cao, L. Guo, M. Dan, et al., Nat. Commun. 12 (2021) 1675.
[57] Y. Liu, S. Shen, J. Zhang, et al., Appl. Surf. Sci. 478 (2019) 762–769.
[58] S. Zhang, L. Wang, C. Liu, et al., Water. Res. 121 (2017) 11–19.
[59] Z. Balta Sayan, N. Görener Erdem, E.Bilgin Simsek, Mater. Chem. Phys. 347 (2026) 131483.
[60] X. Bai, K. An, L. Jia, et al., ACS Appl. Mater. Interfaces. 17 (2025) 36773–36783.
[61] J. Yang, X. Zhang, Z. Zeng, et al., Inorg. Chem. Front. 10 (2023) 6308–6319.
[62] K. Qi, M. Chhowalla, D. Voiry, Mater. Today 40 (2020) 173–192.
[63] E. Zhang, T. Wang, K. Yu, et al., J. Am. Chem. Soc. 141 (2019) 16569–16573.
[64] W. Wang, Y. Li, R. Zhang, et al., Catal. Commun. 12 (2011) 875–879.
[65] H. Chen, K. Shen, J. Chen, et al., J. Mater. Chem. A 5 (2017) 9937–9945.
[66] Y. Chen, Y. Yang, N. Ren, et al., Curr. Opin. Chem. Eng. 41 (2023) 100942.
[67] T. Zhou, J. Deng, Y. Zeng, et al., Small 20 (2024) e2404254.
[68] H. Yang, L. Shang, Q. Zhang, et al., Nat. Commun. 10 (2019) 4585.
[69] S. An, G. Zhang, J. Liu, et al., Chin. J. Catal. 41 (2020) 1198–1207.
[70] H. Chung, D. Cullen, D. Higgins, et al., Science 357 (2017) 479–484.
[71] S. Wei, A. Li, J. Liu, et al., Nat. Nanotechnol. 13 (2018) 856–861.
[72] A. Zitolo, V. Goellner, V. Armel, et al., Nat. Mater. 14 (2015) 937–942.
[73] J. Tuo, Y. Lin, Y. Zhu, et al., Appl. Catal. B 272 (2020) 118960.
[74] S. Ohn, S. Kim, S. Mun, et al., Carbon 124 (2017) 180–187.
[75] M. Mateen, W.C. Cheong, C. Zheng, et al., Chem. Eng. J. 451 (2023) 138305.
[76] K. Kim, T. Kang, M. Kim, et al., Appl. Catal. B 275 (2020) 119107.
[77] H. Zhang, P. An, W. Zhou, et al., Sci. Adv. 4 (2018) eaao6657.
[78] X. Fu, P. Zamani, J.Y. Choi, et al., Adv. Mater. 29 (2017) 1604456.
[79] L. Kumaresan, A. Prabhu, M. Palanichamy, et al., J. Hazard. Mater. 186 (2011) 1183–1192.
[80] J. Tao, M. Wang, G. Liu, et al., J. Adv. Ceram. 11 (2022) 1117–1130.
[81] Z. Zhang, C. Feng, C. Liu, et al., Nat. Commun. 11 (2020) 1215.
[82] X. Yao, X. Hu, Y. Liu, et al., Chemosphere 261 (2020) 127759.
[83] X. Mao, Z. Deng, Y. Liu, et al., Appl. Surf. Sci. 597 (2022) 153625.
[84] X. Tan, H. Li, S. Yang, ChemCatChem 13 (2021) 4859–4877.
[85] T. Sun, H. Jiang, C. Ma, et al., Catal. Commun. 79 (2016) 45–48.
[86] D. Elango, V. Manikandan, J.S. Packialakshmi, et al., Chemosphere 311 (2023) 136983.
[87] L. Shi, X. Ren, Q. Wang, et al., Small 16 (2020) e2002356.
[88] X. Tao, Y. Zhao, S. Wang, et al., Chem. Soc. Rev. 51 (2022) 10120–10122.
[89] S. Chen, T. Takata, K. Domen, Nat. Rev. Mater. 2 (2017) 17050.
[90] J. Cho, N. Suwandaratne, S. Razek, et al., ACS Appl. Mater. Interfaces 12 (2020) 43728–43740.
[91] W. Li, X. Chu, F. Wang, et al., Appl. Catal. B 304 (2022) 121000.
[92] C. Wang, K. Wang, Y. Feng, et al., Adv. Mater. 33 (2021) e2003327.

[93] J. Zhuang, S. Ren, B. Zhu, et al., Chem. Eng. J. 446 (2022) 136873.
[94] J. Guo, Y. Liang, L. Liu, et al., Appl. Surf. Sci. 522 (2020) 146356.
[95] S. Velusamy, A. Roy, S. Sundaram, et al., Chem. Rec. 21 (2021) 1570–1610.
[96] L. Sun, Y. Feng, K. Ma, et al., Appl. Catal. B 306 (2022) 121106.
[97] G. Vilé, P. Sharma, M. Nachtegaal, et al., Sol. RRL 5 (2021) 2100176.
[98] A. Mojiri, J.L. Zhou, H. Ratnaweera, et al., Chemosphere 288 (2022) 132580.
[99] T. Xu, H. Zhao, H. Zheng, et al., Chem. Eng. J. 385 (2020) 123832.
[100] C. Wang, A. Li, C. Li, et al., Adv. Mater. 31 (2019) e1903491.
[101] C. Zhang, D. Qin, Y. Zhou, et al., Appl. Catal. B 303 (2022) 120904.
[102] D.W. Wakerley, M.F. Kuehnel, K.L. Orchard, et al., Nat. Energy 2 (2017) 17021.
[103] Y. Li, G. Lu, S. Li, Chemosphere 52 (2003) 843–850.
[104] D. Wang, Y. Li, G. Li Puma, et al., Appl. Catal. B 168-169 (2015) 25–32.
[105] Y. Cho, H. Kim, S. Lee, et al., J. Catal. 330 (2015) 387–395.
[106] A. Kumar, P. Sharma, G. Sharma, et al., Env. Chem. Lett. 22 (2024) 2405–2424.
[107] X. Li, Y. Liang, W. Li, et al., Mol. Catal. 572 (2025) 114769.
[108] X. Zhang, Z. Cheng, C. Bo, et al., J. Colloid. Interface Sci. 677 (2025) 189–197.
[109] X. Jiang, L. Wang, F. Yu, et al., ACS Sustain. Chem. Eng. 6 (2018) 12695–12705.
[110] S. Liu, X. Zhou, J. Qin, et al., J. Colloid. Interface Sci. 635 (2023) 59–71.
[111] Y. He, Y. Liu, Z. Zhang, et al., Appl. Surf. Sci. 622 (2023) 156911.
[112] H. Liu, C. Xu, D. Li, et al., Angew. Chem. Int. Ed. 57 (2018) 5379–5383.
[113] W. Zhang, Y. Li, C. Wang, et al., Water Res. 47 (2013) 3173–3182.
[114] G. Huang, Z. Xiao, W. Zhen, et al., Water Res. 175 (2020) 115684.